Helsinki University of Technology Institute of Mathematics Research Reports

Espoo 2008 A555

FINITE ELEMENT ANALYSIS OF COMPOSITE PLATES WITH AN APPLICATION TO THE PAPER COCKLING PROBLEM

Juho Könnö **Rolf Stenberg**

TEKNILLINEN KORKEAKOULU
TEKNISKA HÖGSKOLAN
HELSINKI UNIVERSITY OF TECHNOLOGY
TECHNISCHE UNIVERSITÄT HELSINKI
UNIVERSITE DE TECHNOLOGIE D'HELSINKI

Helsinki University of Technology Institute of Mathematics Research Reports
Espoo 2008 A555

FINITE ELEMENT ANALYSIS OF COMPOSITE PLATES WITH AN APPLICATION TO THE PAPER COCKLING PROBLEM

Juho Könnö **Rolf Stenberg**

Helsinki University of Technology
Faculty of Information and Natural Sciences
Department of Mathematics and Systems Analysis

Juho Könnö, Rolf Stenberg: *Finite Element Analysis of Composite Plates with an Application to the Paper Cockling Problem*; Helsinki University of Technology Institute of Mathematics Research Reports A555 (2008).

Abstract: *We present a model for the laminated composite plate problem based on the Reissner-Mindlin model and classical lamination theory. The weak problem based on this model is solved with the finite element method using the MITC finite element family. Detailed a priori estimates are given for the mixed finite element formulation of the problem. Furthermore, we present an application of the theory to the paper cockling problem and investigate the effect of boundary conditions numerically.*

AMS subject classifications: 65N30, 74S05, 74K20

Keywords: Composite plates, MITC, finite element analysis, cockling, paper manufacturing

Correspondence

Juho Könnö
Helsinki University of Technology
Department of Mathematics and Systems Analysis
P.O. Box 1100
FI-02015 TKK
Finland

juho.konno@tkk.fi, rolf.stenberg@tkk.fi

ISBN 978-951-22-9600-2 (print)
ISBN 978-951-22-9601-9 (PDF)
ISSN 0784-3143 (print)
ISSN 1797-5867 (PDF)

Helsinki University of Technology
Faculty of Information and Natural Sciences
Department of Mathematics and Systems Analysis
P.O. Box 1100, FI-02015 TKK, Finland
email: math@tkk.fi http://math.tkk.fi/

1 Introduction

Composite structures are increasingly common in industrial applications due to their desirable properties, such as exceptionally high flexural stiffness-to-weight ratio and structural stability. In fine-grade paper manufacturing controlling the cockling of the paper sheet is of paramount importance. To be able to influence the cockling behavior during the manufacturing process real-time simulations are needed, thus making efficient and reliable numerical solution methods important.

In this work, we present a model for a laminated composite plate based on the classical lamination theory [1], which couples the plate bending problem to a plane elasticity problem. In addition, the laminated composite model can be also applied to modelling sheets of paper. We take a closer look at an application of the classical lamination theory to the paper cockling problem using a recent material model presented in [2]. Reissner-Mindlin kinematic assumptions are used for the plate model. We first formulate the problem by means of minimization of energy. The corresponding weak equations are then discretized by the finite element method using stabilized MITC elements for the plate variables. The in-plane displacements are discretized by standard first order conforming finite elements.

2 The Reissner-Mindlin laminated plate model

The plate bending problem is formulated for a moderately thick plate of thickness t in the domain $\Omega \times (-t/2, t/2)$, where $\Omega \subset \mathbb{R}^2$. The kinematic unknowns are the transverse deflection w, the rotation of the normals $\boldsymbol{\beta}$ and the in-plane displacement $\boldsymbol{u}$. The plate is subjected to two types of loading, namely in-plane loading $\boldsymbol{f}$ and transverse loading g. In composite materials the connection between the planar elasticity problem and the plate bending problem is introduced directly through the constitutive equations. In the following, both dyadic and index notation for tensors are used in parallel. Indices in Greek letters take the values $\{1, 2\}$ and those in Roman letters the values $\{1, 2, 3\}$.

2.1 Constitutive relations for a single layer

In the following, all quantities with a tilde are always in the ply coordinate system, whereas those without are in the global coordinate system. The second-order transformation tensor T_{ij} is defined by the rotation angle ϕ of the ply coordinate system as follows

$$T = \begin{pmatrix} \cos\phi & -\sin\phi \\ \sin\phi & \cos\phi \end{pmatrix}. \tag{1}$$

For a single layer, the constitutive tensor, along with the stress and strain tensors, must be transformed from the ply coordinate system to the global

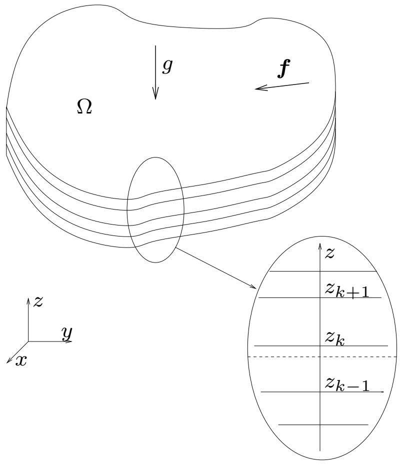

Figure 1: Structure of the composite plate

coordinate system. In index notation, the transformation for the constitutive tensor is

$$C_{ijkl} = T_{ip}T_{jq}T_{kr}T_{ls}\tilde{C}_{pqrs}. \tag{2}$$

For the stresses and strains it holds

$$\sigma_{ij} = T_{ip}T_{jq}\tilde{\sigma}_{pq}, \quad \epsilon_{ij} = T_{ip}T_{jq}\tilde{\epsilon}_{pq}. \tag{3}$$

The constitutive equation for a single ply in the ply coordinate system is

$$\tilde{\sigma} = \tilde{\boldsymbol{C}} : \tilde{\boldsymbol{\varepsilon}}. \tag{4}$$

The non-zero components of the constitutive tensor in the ply coordinate system are defined by the six independent engineering parameters E_1, E_2, ν_{12}, G_{12}, G_{23}, and G_{31} as [3, 4]

$$\begin{array}{ll} C_{1111} = E_1/(1-\nu_{12}\nu_{21}), & C_{2222} = E_2/(1-\nu_{12}\nu_{21}), \\ C_{1122} = \nu_{12}E_2/(1-\nu_{12}\nu_{21}), & C_{1212} = G_{12}, \\ C_{2323} = G_{23}, & C_{3131} = G_{31}. \end{array} \tag{5}$$

2.2 Kinematic relations

We denote by $\boldsymbol{\varepsilon}(\boldsymbol{u}) := \frac{1}{2}(\nabla\boldsymbol{u}+\nabla\boldsymbol{u}^T)$ the linear strain tensor. In the Reissner-Mindlin laminate model we allow a constant shear deformation in the thickness direction of the plate, and take into account the strain induced by the in-plane displacements. The kinematic relations in the global coordinate system using the Reissner-Mindlin kinematic assumptions are [5]

$$\epsilon_{\alpha\beta} = \epsilon_{\alpha\beta}(\boldsymbol{u}) + z\epsilon_{\alpha\beta}(\boldsymbol{\beta}), \tag{6}$$

$$\epsilon_{3\alpha} = \frac{\partial w}{\partial x_\alpha} - \beta_\alpha, \tag{7}$$

$$\epsilon_{33} = 0. \tag{8}$$

2.3 Constitutive relations for the plate

Having now formed the constitutive relations for a single layer, we must form the constitutive tensor for the whole laminate. First, we form the membrane and shear stress resultants $\boldsymbol{N}$ and $\boldsymbol{S}$, along with the bending moment resultant $\boldsymbol{M}$, by integrating over the thickness of the laminate. $\boldsymbol{C}_k$ is the constitutive tensor for a single ply. The structure of the laminate is depicted in Figure 1. With this notation the force resultants for a laminate with n layers read

$$N_{\alpha\beta} = \int_{-t/2}^{t/2} \sigma_{\alpha\beta} dz = \sum_{k=1}^{n} \int_{z_{k-1}}^{z_k} \sigma_{\alpha\beta} dz, \tag{9}$$

$$M_{\alpha\beta} = \int_{-t/2}^{t/2} \sigma_{\alpha\beta} z dz = \sum_{k=1}^{n} \int_{z_{k-1}}^{z_k} \sigma_{\alpha\beta} z dz, \tag{10}$$

$$S_{\alpha} = \int_{-t/2}^{t/2} \sigma_{3\alpha} dz = \sum_{k=1}^{n} \int_{z_{k-1}}^{z_k} \sigma_{3\alpha} dz. \tag{11}$$

We also assume individual layers to be homogeneous in the thickness direction. Inserting the kinematic relations (6)-(8) we can write the stress and moment resultants with the help of the following second- and fourth-order tensors [4]

$$A_{\alpha\beta\gamma\delta} = \sum_{k=1}^{n} \int_{z_{k-1}}^{z_k} C_{\alpha\beta\gamma\delta} dz = \sum_{k=1}^{n} (z_k - z_{k-1}) C^k_{\alpha\beta\gamma\delta}, \tag{12}$$

$$B_{\alpha\beta\gamma\delta} = \sum_{k=1}^{n} \int_{z_{k-1}}^{z_k} C_{\alpha\beta\gamma\delta} z dz = \frac{1}{2} \sum_{k=1}^{n} (z_k^2 - z_{k-1}^2) C^k_{\alpha\beta\gamma\delta}, \tag{13}$$

$$D_{\alpha\beta\gamma\delta} = \sum_{k=1}^{n} \int_{z_{k-1}}^{z_k} C_{\alpha\beta\gamma\delta} z^2 dz = \frac{1}{3} \sum_{k=1}^{n} (z_k^3 - z_{k-1}^3) C^k_{\alpha\beta\gamma\delta}, \tag{14}$$

$$A^*_{\alpha\beta} = \sum_{k=1}^{n} \int_{z_{k-1}}^{z_k} C_{3\alpha3\beta} dz = \sum_{k=1}^{n} (z_k - z_{k-1}) C^k_{3\alpha3\beta}. \tag{15}$$

With these definitions the resultants can be written as

$$\boldsymbol{N} = \boldsymbol{A} \colon \boldsymbol{\varepsilon}(\boldsymbol{u}) + \boldsymbol{B} \colon \boldsymbol{\varepsilon}(\boldsymbol{\beta}), \tag{16}$$

$$\boldsymbol{M} = \boldsymbol{B} \colon \boldsymbol{\varepsilon}(\boldsymbol{u}) + \boldsymbol{D} \colon \boldsymbol{\varepsilon}(\boldsymbol{\beta}), \tag{17}$$

$$\boldsymbol{S} = \boldsymbol{A}^* \cdot (\nabla w - \boldsymbol{\beta}). \tag{18}$$

2.4 The Reissner-Mindlin plate model

The energy associated with each deformation mode can be computed by first multiplying each strain component with the corresponding stress resultant, and then integrating over the domain Ω occupied by the plate. We introduce the following scaling for the variables, material tensors and loadings:

$$\begin{cases} \boldsymbol{u} \to \frac{1}{t}\boldsymbol{u}, \\ \boldsymbol{\beta} \to \boldsymbol{\beta}, \\ w \to w \end{cases}, \quad \begin{cases} \boldsymbol{A} \to \frac{1}{t}\boldsymbol{A}, \\ \boldsymbol{B} \to \frac{1}{t^2}\boldsymbol{B}, \\ \boldsymbol{D} \to \frac{1}{t^3}\boldsymbol{D}, \\ \boldsymbol{A}^* \to \frac{1}{t}\boldsymbol{A}^* \end{cases}, \quad \begin{cases} \boldsymbol{f} \to \frac{1}{t^2}\boldsymbol{f}, \\ g \to \frac{1}{t^3}g \end{cases}. \tag{19}$$

By scaling the unknowns as above, the total energy is scaled by a factor of t^3. The scaled total energy of the plate can be written as [6]

$$\begin{aligned} \Pi(\boldsymbol{u}, w, \boldsymbol{\beta}) =& \frac{1}{2}\int_\Omega \boldsymbol{\varepsilon}(\boldsymbol{u}) \colon \boldsymbol{A} \colon \boldsymbol{\varepsilon}(\boldsymbol{u}) d\Omega \\ &+ \int_\Omega \boldsymbol{\varepsilon}(\boldsymbol{u}) \colon \boldsymbol{B} \colon \boldsymbol{\varepsilon}(\boldsymbol{\beta}) d\Omega \\ &+ \frac{1}{2}\int_\Omega \boldsymbol{\varepsilon}(\boldsymbol{\beta}) \colon \boldsymbol{D} \colon \boldsymbol{\varepsilon}(\boldsymbol{\beta}) d\Omega \\ &+ \frac{1}{2t^2}\int_\Omega (\nabla w - \boldsymbol{\beta}) \cdot \boldsymbol{A}^* \cdot (\nabla w - \boldsymbol{\beta}) d\Omega \\ &- \int_\Omega \boldsymbol{f} \cdot \boldsymbol{u} d\Omega - \int_\Omega g w d\Omega. \end{aligned} \tag{20}$$

The scaled shear force $\boldsymbol{q}$ is

$$\boldsymbol{q} = t^{-2}\boldsymbol{A}^* \cdot (\nabla w - \boldsymbol{\beta}). \tag{21}$$

The shear force plays a key role in the error analysis of the associated finite element method. In the analysis we treat the shear force as an independent unknown thus arriving at a mixed formulation for the original problem.

2.5 Weak form of the equations

To derive the associated weak form of the problem we minimize the energy expression (20) with respect to the kinematic variables. The problem is: Find $(\boldsymbol{u}, w, \boldsymbol{\beta}) \in \boldsymbol{U} \times W \times \boldsymbol{V}$ such, that

$$(\boldsymbol{A} \colon \boldsymbol{\varepsilon}(\boldsymbol{u}), \boldsymbol{\varepsilon}(\boldsymbol{v})) + (\boldsymbol{B} \colon \boldsymbol{\varepsilon}(\boldsymbol{v}), \boldsymbol{\varepsilon}(\boldsymbol{\beta})) = (\boldsymbol{f}, \boldsymbol{v}) \quad \forall \boldsymbol{v} \in \boldsymbol{U}$$

and

$$\begin{aligned} &(\boldsymbol{B} \colon \boldsymbol{\varepsilon}(\boldsymbol{u}), \boldsymbol{\varepsilon}(\boldsymbol{\eta})) + (\boldsymbol{D} \colon \boldsymbol{\varepsilon}(\boldsymbol{\beta}), \boldsymbol{\varepsilon}(\boldsymbol{\eta})) \\ &\qquad + t^{-2}(\boldsymbol{A}^* \cdot (\nabla w - \boldsymbol{\beta}), (\nabla \omega - \boldsymbol{\eta})) = (g, \omega), \quad \forall (\omega, \boldsymbol{\eta}) \in W \times \boldsymbol{V}. \end{aligned}$$

The minimization results in two equations, a standard plane elasticity problem and a Reissner-Mindlin plate problem. The two problems are coupled by an additional term connecting the rotational and the in-plane degrees of freedom through the tensor $\boldsymbol{B}$. $\boldsymbol{U} \subset [H^1(\Omega)]^2, W \subset H^1(\Omega)$ and $\boldsymbol{V} \subset [H^1(\Omega)]^2$ are suitably chosen variational spaces, see e.g. [7, 8].

2.6 Coercivity result

We prove a coercivity result similar to the one presented in [6]. We extend the proof by not assuming the plate to be evenly distributed into plies of thickness $\frac{t}{n}$, and present explicit relations for the coercivity and continuity constants.

Theorem 1. *There exists positive constants C_1, C_2 such that for every pair of symmetric tensors $\boldsymbol{\tau}, \boldsymbol{\sigma} \in [L^2(\Omega)]^4$ it holds*

$$C_1(\|\boldsymbol{\tau}\|_0^2 + \|\boldsymbol{\sigma}\|_0^2) \leq (\boldsymbol{A} \colon \boldsymbol{\tau}, \boldsymbol{\tau}) + 2(\boldsymbol{B} \colon \boldsymbol{\tau}, \boldsymbol{\sigma}) + (\boldsymbol{D} \colon \boldsymbol{\sigma}, \boldsymbol{\sigma}) \leq C_2(\|\boldsymbol{\tau}\|_0^2 + \|\boldsymbol{\sigma}\|_0^2), \tag{22}$$

in which $\boldsymbol{A}, \boldsymbol{B}, \boldsymbol{D}$ are the tensors defined above, and it is assumed that the constitutive tensor $\boldsymbol{C} \in [L^2(\Omega)]^{4\times 4}$ and is symmetric positive definite. Furthermore, denoting by δ the ratio of the thickness of the thinnest layer to the thickness of the whole laminate, $\delta = \frac{1}{t}\min_k h_k$, we have $C_1 \sim n\delta^3$ and $C_2 \sim 1$.

Proof. Writing the expression as a formal matrix product and taking into account that $\boldsymbol{B}$ is symmetric we have

$$(\boldsymbol{A} \colon \boldsymbol{\tau}, \boldsymbol{\tau}) + 2(\boldsymbol{B} \colon \boldsymbol{\tau}, \boldsymbol{\sigma}) + (\boldsymbol{D} \colon \boldsymbol{\sigma}, \boldsymbol{\sigma}) = (\begin{bmatrix} \boldsymbol{\tau} \\ \boldsymbol{\sigma} \end{bmatrix}, \sum_{k=1}^{n} \begin{bmatrix} \boldsymbol{A}_k & \boldsymbol{B}_k \\ \boldsymbol{B}_k & \boldsymbol{D}_k \end{bmatrix} \begin{bmatrix} \boldsymbol{\tau} \\ \boldsymbol{\sigma} \end{bmatrix}). \tag{23}$$

Thus the theorem is true, if the coefficient matrix is bounded and positive definite. Turning our attention to the matrix for a single ply, we use definitions (12)–(14) to write the corresponding matrix in the form

$$\begin{bmatrix} \boldsymbol{A}_k & \boldsymbol{B}_k \\ \boldsymbol{B}_k & \boldsymbol{D}_k \end{bmatrix} = \begin{bmatrix} \frac{1}{t}(z_k - z_{k-1}) & \frac{1}{2t^2}(z_k^2 - z_{k-1}^2) \\ \frac{1}{2t^2}(z_k^2 - z_{k-1}^2) & \frac{1}{3t^3}(z_k^3 - z_{k-1}^3) \end{bmatrix} \begin{bmatrix} \boldsymbol{C}_k & 0 \\ 0 & \boldsymbol{C}_k \end{bmatrix} \tag{24}$$

Since the last matrix is block diagonal, the product of these two matrices commutes. Thus, it is sufficient to prove the positive definiteness property for both matrices separately.

The tensor $\boldsymbol{C}_k$ is symmetric and positive definite by definition, hence we only need to know the eigenvalues of the 2×2 matrix

$$R_k := \begin{bmatrix} \frac{1}{t}(z_k - z_{k-1}) & \frac{1}{2t^2}(z_k^2 - z_{k-1}^2) \\ \frac{1}{2t^2}(z_k^2 - z_{k-1}^2) & \frac{1}{3t^3}(z_k^3 - z_{k-1}^3) \end{bmatrix}. \tag{25}$$

The eigenvalues of a R_k are [9]

$$\lambda_1(R_k) = \frac{\operatorname{tr}(R_k)}{2}\left(1 - \sqrt{1 - \frac{4\det(R_k)}{\operatorname{tr}(R_k)^2}}\right),$$

$$\lambda_2(R_k) = \frac{\operatorname{tr}(R_k)}{2}\left(1 + \sqrt{1 - \frac{4\det(R_k)}{\operatorname{tr}(R_k)^2}}\right).$$

For matrix R_k the determinant and the trace can be written as

$$\begin{aligned}
\det(R_k) &= \frac{1}{3t^4}(z_k^3 - z_{k-1}^3)(z_k - z_{k-1}) - \frac{1}{4t^4}(z_k^2 - z_{k-1}^2)^2 = \frac{1}{12t^4}(z_k - z_{k-1})^4, \\
\operatorname{tr}(R_k) &= \frac{1}{t}(z_k - z_{k-1}) + \frac{1}{3t^3}(z_k^3 - z_{k-1}^3).
\end{aligned}$$

Denoting the thickness of the k:th ply by $h_k = z_k - z_{k-1}$ the determinant reads

$$\det(R_k) = \frac{h_k^4}{12t^4} > 0,$$

and for the trace it holds

$$\operatorname{tr}(R_k) \geq \frac{1}{t}(z_k - z_{k-1}) = \frac{h_k}{t} > 0.$$

The eigenvalues are real and positive since

$$0 < \frac{4\det(R_k)}{\operatorname{tr}(R_k)^2} \leq \frac{h_k^2}{3t^2} < 1.$$

For every k it holds $z_k \in [-t/2, t/2]$. Thus we can estimate the trace from above by

$$\operatorname{tr}(R_k) = \frac{1}{t}(z_k - z_{k-1}) + \frac{1}{3}((\frac{z_k}{t})^3 - (\frac{z_{k-1}}{t})^3) \leq \frac{2}{t}(z_k - z_{k-1}) = \frac{2h_k}{t}.$$

Using the inequality $1 - \sqrt{1-x} \geq \frac{x}{2},\ x \in [0,1]$, we have for the smallest eigenvalue

$$\lambda_1(R_k) \geq \frac{\operatorname{tr}(R_k)}{2}\frac{2\det(R_k)}{\operatorname{tr}(R_k)^2} = \frac{h_k^3}{24t^3}.$$

By Weyl's inequality [9]

$$\lambda_1(\sum_{k=0}^{n} R_k) \geq \sum_{k=0}^{n} \lambda_1(R_k) = \frac{1}{24t^3}\sum_{k=0}^{n} h_k^3 \geq \frac{n\delta^3}{24}. \tag{26}$$

For the largest eigenvalue we have

$$\lambda_2(\sum_{k=0}^{n} R_k) \leq \sum_{k=0}^{n} \lambda_2(R_k) \leq \sum_{k=0}^{n} \operatorname{tr}(R_k) = \frac{1}{t}(z_n - z_0) + \frac{1}{3t^3}(z_n^3 - z_0^3) = \frac{13}{12}. \tag{27}$$

Thus the matrix is uniformly bounded from above, and the constant C_2 is completely independent of the ply configuration of the laminate. The lower bound, on the other hand, is related to the thickness ratio δ as $C_1 \sim n\delta^3$. $\square$

3 The finite element model

In the finite element formulation we use the well-known MITC elements of the first order as presented in [10, 8]. In the MITC family of elements, the locking phenomenon is avoided by projecting the rotation $\boldsymbol{\beta}$ onto a suitable subspace of $H(\mathrm{rot}, \Omega)$ using the reduction operator $\boldsymbol{R}_h$ defined below [8]. Using linear MITC elements requires a modification of the energy expression to achieve a stable method. The stabilization is obtained by locally replacing the factor t^{-2} by $(t+\alpha h_K)^{-2}$ in the shear energy expression [11], in which h_K is the local mesh parameter and α a suitably chosen stabilization parameter, typically $\alpha = 0.1$. For higher order elements additional terms are required in the bilinear form for the stabilization when using equal order interpolation. However, an equivalent way is to use additional inner degrees of freedom for the rotation and the non-modified bilinear form [12]. For simplicity, we present the element spaces and convergence results only for the first-order elements. For details on higher order elements, see [7, 10, 8].

3.1 Implementation

We denote by $\mathcal{K}_h$ a shape-regular quadrilateral mesh over the domain Ω. The finite element spaces for quadrilateral first-order elements are

$$\begin{aligned}
\boldsymbol{V}_h &= \{\boldsymbol{\eta} \in \boldsymbol{V} \mid \boldsymbol{\eta}|_K \in [Q_1(K)]^2, \forall K \in \mathcal{K}_h\},\\
W_h &= \{w \in W \mid w|_K \in Q_1(K), \forall K \in \mathcal{K}_h\},\\
\boldsymbol{U}_h &= \{\boldsymbol{u} \in \boldsymbol{U} \mid \boldsymbol{u}|_K \in [Q_1(K)]^2, \forall K \in \mathcal{K}_h\}.
\end{aligned}$$

The discrete space $\boldsymbol{\Gamma}_h$ for the shear force is defined on the reference element $\hat{K}$ as

$$\boldsymbol{\Gamma}_h(\hat{K}) = \{\hat{\boldsymbol{s}} = (\hat{s}_1, \hat{s}_2) |\ \hat{s}_1 = a + b\hat{x}_2,\ \hat{s}_2 = c + d\hat{x}_1,\ \text{for some } a, b, c, d \in \mathbb{R}\}.$$

We define for each element $K \in \mathcal{K}_h$ the shear space as

$$\boldsymbol{\Gamma}_h(K) = \{\boldsymbol{s} = (s_1, s_2) |\ \boldsymbol{s}(x, y) = \boldsymbol{J}_K^{-T} \hat{\boldsymbol{s}}(\boldsymbol{F}_K^{-1}(x, y)),\ \text{for some } \hat{\boldsymbol{s}} \in \boldsymbol{\Gamma}_h(\hat{K})\}.$$

Here $\boldsymbol{F}_K$ is the mapping from the reference element $\hat{K}$ to the element K, and $\boldsymbol{J}_K$ the corresponding Jacobian matrix. This allows us to define the reduction operator $\boldsymbol{R}_h : \boldsymbol{V}_h \to \boldsymbol{\Gamma}_h(K)$ from the following conditions on the edges E of each element

$$\int_E ((\boldsymbol{R}_h \boldsymbol{s} - \boldsymbol{s}) \cdot \boldsymbol{\tau}) = 0.$$

Here $\boldsymbol{\tau}$ is the tangent to each edge E of the element K.

For the reduction operator it holds $\boldsymbol{R}_h \nabla w = \nabla w$ [8]. Thus the discrete formulation for the problem is: Find $(\boldsymbol{u}_h, w_h, \boldsymbol{\beta}_h) \in \boldsymbol{U}_h \times W_h \times \boldsymbol{V}_h$ such that it holds

$$(\boldsymbol{A} \colon \boldsymbol{\varepsilon}(\boldsymbol{u}_h), \boldsymbol{\varepsilon}(\boldsymbol{v}_h)) + (\boldsymbol{B} \colon \boldsymbol{\varepsilon}(\boldsymbol{v}_h), \boldsymbol{\varepsilon}(\boldsymbol{\beta}_h)) = (\boldsymbol{f}, \boldsymbol{v}_h) \quad \forall \boldsymbol{v}_h \in \boldsymbol{U}_h$$

and

$$
\begin{aligned}
&(\boldsymbol{B}\colon \boldsymbol{\varepsilon}(\boldsymbol{u}_h), \boldsymbol{\varepsilon}(\boldsymbol{\eta}_h)) + (\boldsymbol{D}\colon \boldsymbol{\varepsilon}(\boldsymbol{\beta}_h), \boldsymbol{\varepsilon}(\boldsymbol{\eta}_h)) \\
&\qquad + \sum_{K\in\mathcal{K}} \frac{1}{t^2+\alpha h_K^2}(\boldsymbol{A}^*\cdot(\nabla w_h - \boldsymbol{R}_h\boldsymbol{\beta}_h), (\nabla \omega_h - \boldsymbol{R}_h\boldsymbol{\eta}_h)) = (g, \omega_h) \\
&\qquad\qquad\qquad\qquad\qquad\qquad\qquad\qquad \forall(\omega_h, \boldsymbol{\eta}_h) \in W_h \times \boldsymbol{V}_h.
\end{aligned}
$$

3.2 Theoretical considerations

Generally speaking, all results for the standard Reissner-Mindlin plate can be extended to the case of a laminated plate. The norm equivalence in Theorem 1 is essential in proving the convergence properties. It shows that the coupled equation is elliptic with respect to all the kinematic variables involved and the upper bound does not depend on the ply structure of the laminate. Thus we can show that the laminated Reissner-Mindlin plate model has the same desirable convergence properties as the homogeneous plate [6, 13, 11] by considering both parts of the equation separately and using Theorem 1. The regularity estimates needed in the analysis can be found in [7, 14, 13]. For the plate model not involving the in-plane displacements we use a stability-consistency type argument. The stability property only holds in a specific mesh dependent norm, see [7]. Furthermore, using a mesh-stabilized method induces a consistency error due to the stabilizing term in the discrete bilinear form. The consistency error can be bouded from above by the weighted norm of the shear force $\boldsymbol{q}$. For the plane elasticity problem the estimates follow from the classical theory of finite element methods [15].

The main convergence result gives us convergence relative h in the domain Ω, where h is the global mesh parameter. More precisely, one has the following *a priori* error estimate for the coupled problem with a sufficiently smooth solution

$$
\|\boldsymbol{\beta}-\boldsymbol{\beta}_h\|_1 + \|w-w_h\|_1 + t\|\boldsymbol{q}-\boldsymbol{q}_h\|_0 + \|\boldsymbol{q}-\boldsymbol{q}_h\|_{-1} + \|\boldsymbol{u}-\boldsymbol{u}_h\|_1 \le Ch.
$$

Here the constant C depends only on the loading.

4 Modelling paper with the plate model

In general, paper is a very inhomogeneous material with arbitrary fiber directions and strong anisotropies. However, a valid simplification is to consider a sheet of paper as a material composed of layers with individual fiber direction patterns, defined by the angle $\Theta = \frac{\pi}{2} - \phi$ in each individual data block. The second local material parameter needed to describe the material is the level of local anisotropy denoted by ξ. In addition, only the easily measurable global Young's modulus E and poisson number ν are needed. The definitions of the local quantities Θ and ξ are presented in Figure 2.

The level of anisotropy ξ is defined as the ratio of the largest fiber concentration to the concentration in the direction perpendicular to it. This can be

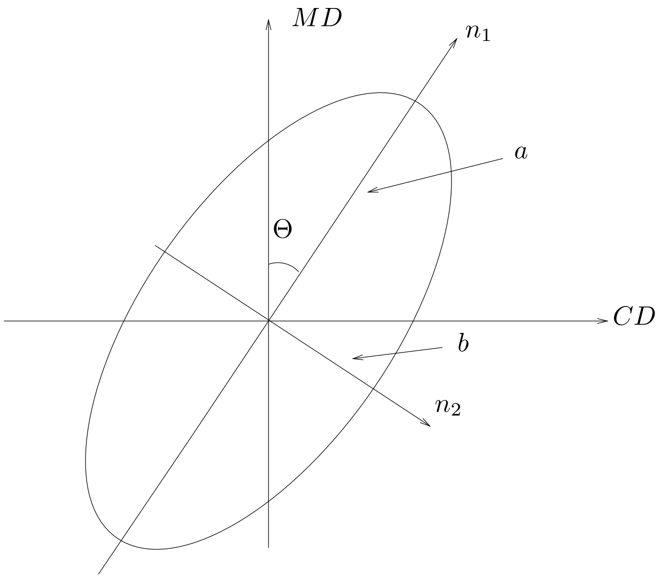

Figure 2: Definition of the orientation angle Θ and anisotropy ξ. MD is the machine direction and CD the cross-machine direction. The n_1 axis points in the direction of strongest anisotropy, and n_2 is perpendicular to this direction.

interpreted geometrically as the ratio of the pricipal axes of the ellipsoid in Figure 2, namely $\xi = a/b$. Some practical methods for measuring the angle and anisotropy data from a paper sample are presented in [2, 16]. The third local parameter needed for the model is the moisture percentage β, which is allowed to vary not only in the data blocks, but also layerwise in the thickness direction, which is mostly the case in the actual modelled situations. The following model for the linear and elastic cockling of paper is presented originally in [2].

4.1 Young's modulus and Poisson ratio

In practice, only the global Young's moduli E_{MD} and E_{CD} are usually measured from a paper sample. The local Young's moduli in the ply coordinate system are derived from these two quantities, assuming they depend only on the moisture level β and anisotropy ξ. By geometric inspection and the definition of ξ, it evidently holds

$$\frac{E_1}{E_2} = \xi. \tag{28}$$

Since the geometric mean $E = \sqrt{E_1 E_2}$ of the Young's moduli remains approximately constant regardless of the orientation, we can write the local moduli in the following form treating the geometric mean as an invariant

$$E_1 = E\sqrt{\xi}, \qquad E_2 = \frac{E}{\sqrt{\xi}}. \tag{29}$$

Empirical results show [2, 17], that for most paper qualities the moisture dependence of the geometric average E is linear. In this paper we use the dependence presented in [2],

$$E = (-0.25\beta + 6.5) \text{ GPa}. \tag{30}$$

The Poisson ratios are defined from the global quantities with the help of the local Young's moduli. By Maxwell's reciprocal relation it holds

$$\frac{\nu_{12}}{\nu_{21}} = \frac{E_1}{E_2} = \xi. \tag{31}$$

From this we have analogously to the previous case

$$\nu_{12} = \nu\sqrt{\xi}, \quad \nu_{21} = \frac{\nu}{\sqrt{\xi}}. \tag{32}$$

Once again, experiments support the fact that the global Poisson number depends linearly on the moisture content for the majority of paper qualities, as noted in [2] and the references therein. Here the following dependence is used

$$\mu = 0.015\beta + 0.150. \tag{33}$$

The shear modulus is finally defined analoguously to isotropic materials [2, 13] from the geometric averages E and ν. Thus we get the following expression not depending on the local anisotropy ξ:

$$G_{12} = \frac{E}{2(1+\mu)} = \frac{6.5 - 0.25\beta}{2.3 + 0.03\beta} \text{ GPa}. \tag{34}$$

The model used here is also consistent with the isotropic case, since for homogeneous material the anisotropy $\xi = 1$. In this case we have $E_1 = E_2 = E$, and $\nu_{12} = \nu_{21} = \nu$, as expected. For G_{13} and G_{23} we use the reference values from [2].

4.2 Moisture loading

The primary source of loading during the drying process is the shrinking of the paper with dropping moisture level. The shrinking phenomenon can be modelled mathematically exactly in the same way as heat expansion, with the moisture expansion coefficients depending on the local anisotropy ξ as follows:

$$\alpha_1(\xi) = 0.0006 - 0.00015\sqrt{\xi - 1}, \tag{35}$$

$$\alpha_2(\xi) = 0.0006 + \sqrt{7 \times 10^{-8}(\xi - 1)}. \tag{36}$$

These are values for a typical paper sample taken from [2]. The corresponding strain is obtained from the coefficients as

$$\epsilon_{ij}^{\text{moisture}} = \begin{pmatrix} \alpha_1(\xi)\beta & 0 \\ 0 & \alpha_2(\xi)\beta \end{pmatrix}. \tag{37}$$

As with heat expansion, the shrinking only induces strains in the principal ply coordinate directions. However, globally we get also shear deformations as the strains and corresponding stresses are transferred from the ply coordinate system to the global coordinate system. The moisture content β is allowed to vary from layer to layer. Moreover, this causes no mathematical problems since the induced stress is computed layerwise.

4.3 Boundary conditions

For the in-plane displacement $\boldsymbol{u}$ assigning the boundary conditions is straighforward. The Reissner-Mindlin plate model, on the other hand, accounts for a variety of different boundary conditions. We denote by $\boldsymbol{\beta_n}$ and $\boldsymbol{\beta_\tau}$ the rotations in the normal and tangent directions of the boundary, respectively. On each boundary we can set one of the following physically sound boundary conditions for the plate variables $(w, \boldsymbol{\beta})$ [5]:

- Clamped, fixing w and both components of $\boldsymbol{\beta}$
- Soft clamped, fixing w and $\boldsymbol{\beta}_n$
- Simply supported, fixing only w
- Hard simply supported, fixing w and $\boldsymbol{\beta_\tau}$
- Free, no restrictions on the variables

The actual boundary conditions in the paper machine during the manufacturing process are problematic to model accurately. Since no large scale curving usually occurs during the process, the natural choice is to set $w = 0$ on all edges. We take a closer look at choosing the correct boundary conditions for the plate and in-plane variables in the numerical experiments below.

5 Numerical tests

In the numerical experiments, we concentrate on the effect of different boundary conditions on the cockling behaviour of the paper sheet. All tests were performed on a 192×192 square mesh with first order stabilized MITC4 [11] elements. In the results, we filter out the lowest 20 percent of wavelengths. A relatively low-order high-pass filter based on Fourier transform techniques is used. Filtering is used to focus on the local shape of the cockles instead of the large-scale deformations of the paper sheet. The size of the simulated paper sample is 1000 mm $\times$ 1000 mm in all of the computations. All results are presented in millimetres. The computations were performed with the commercial Numerrin software [18], in which the elements presented are implemented.

5.1 Effect of different boundary conditions

In the numerical experiments we consider the two most important boundary conditions for the Reissner-Mindlin model, namely simply supported and clamped boundaries. Furthermore, we have additional boundary conditions for the in-plane displacements. Here we consider either unconstrained or completely fixed planar displacements. The aim of these numerical experiments is to find out which boundary conditions affect the cockling behavior the most, and thus the choice of which plays the most prominent role in the modelling process. The resulting cockling behavior for these four cases is presented in Figures 3 and 4.

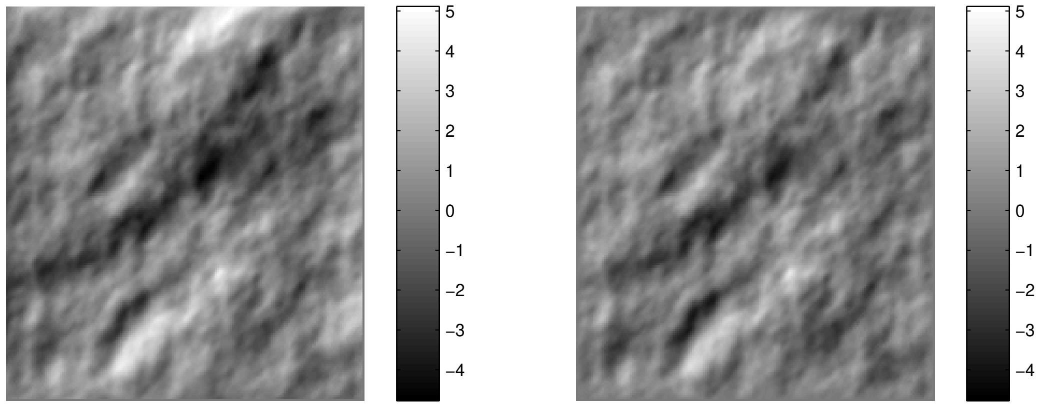

Figure 3: Cockling behavior with unconstrained planar displacements. On the left we have simply supported boundary conditions and on the right clamped boundary conditions.

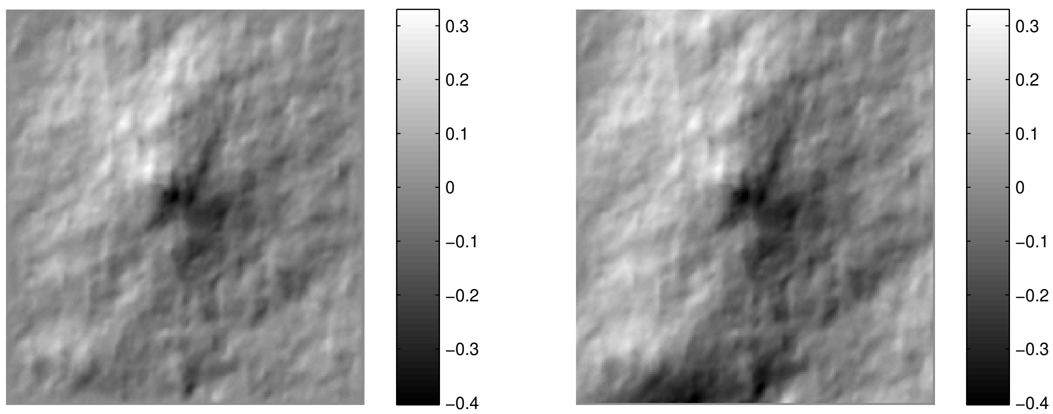

Figure 4: Cockling behavior with constrained planar displacements. On the left we have simply supported boundary conditions and on the right clamped boundary conditions.

As is evident from the results, different boundary conditions for the planar displacements give completely different cockling behaviour. With the unconstrained boundary conditions the amplitude of the cockling is roughly a decade larger than for the constrained case. Thus choosing the boundary condition for the planar diplacements seems to play the most crucial role. This can be explained by considering the moisture expansion behaviour of the laminate. Since the in-plane displacements $\boldsymbol{u}$ and rotations $\boldsymbol{\beta}$ are coupled, fixing the in-plane displacements induces moment loadings on the laminate accounting for larger and smoother total bending of the plate.

Next we consider the choice of boundary condition for the plate variables w and $\boldsymbol{\beta}$. From Figure 5 we can see, that large values of absolute difference between the solutions are concentrated near the boundaries, whereas in the rest of the domain the difference is rather smooth. This suggest that the choice of the boundary condition for the plate equation has less signifigance than the choice for the in-plane displacements, since the overall local cockling behaviour and the amplitude of the cockles is virtually unchanged.

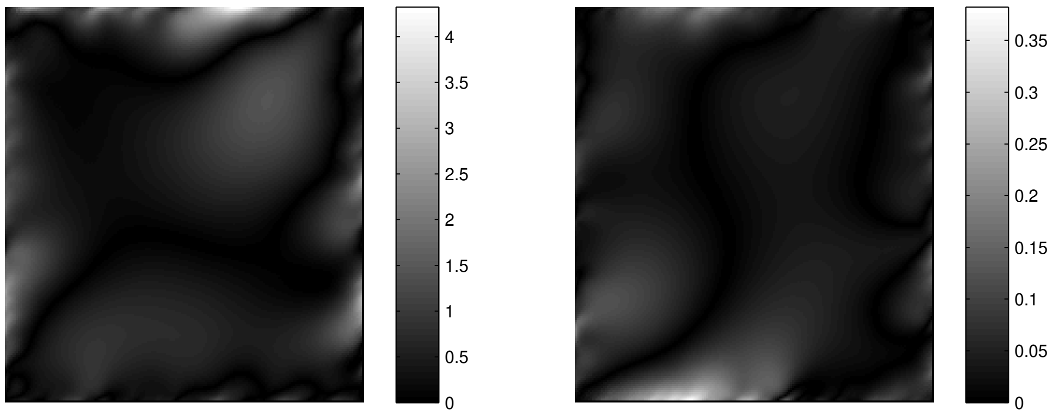

Figure 5: The absolute difference between the simply supported and clamped solution for unconstrained planar displacements on the left, and for the constrained case on the right.

5.2 Effect of mesh density

In order to validate the method, different mesh densities were tested. For the test case simply supported and unrestricted boundary conditions were chosen. We use three different square meshes, sized 48×48, 96×96, and 192×192 elements. The material data is represented on a rectangular 96×96 grid. On the coarsest mesh both first- and second-order elements are used, whereas on the denser meshes only linear elements are considered. Linear elements use mesh stabilization, the second-order elements are stabilized via additional internal rotational degrees of freedom [8, 10]. The error compared to the solution on the finest mesh is presented in Figures 6 and 7.

As can be seen from the results, the difference between one or four elements per data area is rather small. On the coarser mesh the method instead fails to catch the details of the solution. This is natural, since we have discontinuous material parameters inside each element. Using second-order elements does not remedy the situation, and seems to offer no real advantage since the number of degrees of freedom is larger than for the first-order elements on the denser mesh. The same phenomenon appears both in the raw and filtered data. Thus the preferable method seems to be using linear stabilized elements on a dense enough mesh, since both the material data and the solution are highly irregular.

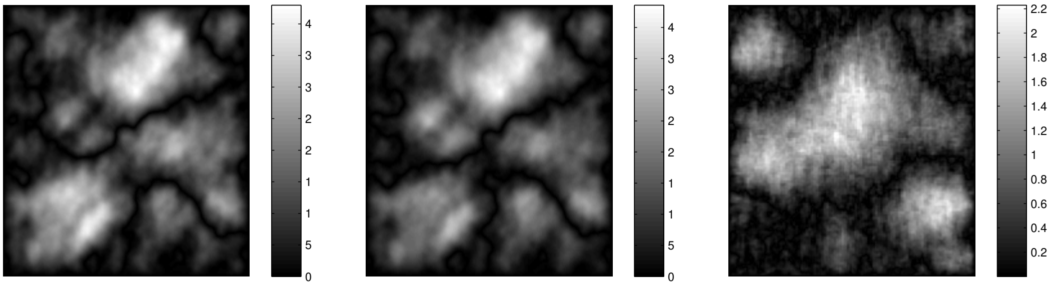

Figure 6: The relative error with respect to the solution on the finest mesh in percent. From left to right: first order elements on 48×48 mesh, second order elements on 48×48 mesh, and first order elements on 96×96 mesh.

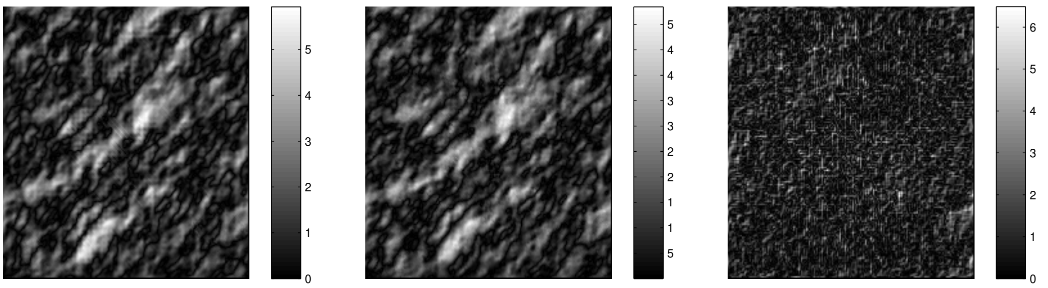

Figure 7: The relative error with respect to the solution on the finest mesh in percent with the filtering of the lowest 20 percent of wavelengths applied to the solution. Figures ordered from left to right as above.

6 Concluding remarks

We noticed that the laminate model based on classical lamination theory and Reissner-Mindlin kinematic assumptions is well-defined and inherits the convergence properties from those of plane elasticity and Reissner-Mindlin plate theory. It also appears to be quite well-suited to modelling the paper cockling phenomenon using the material model presented in [2]. The model also allows relatively straightforward implementation of more advanced material models as proposed in [16]. We were also able to determine the signifigance of different boundary conditions on the cockling phenomenon, and identified the choice of boundary condition for the in-plane displacements to be the crucial factor in the model. Finally, it seems reasonable to use first-order elements one a fine mesh, since second-order elements seem to offer no obvious advantage with very irregular material data.

References

[1] J.N. Reddy. *Mechanics of Laminated Composite Plates and Shells*. CRC Press, 2004.

[2] Teemu Leppänen. *Effect of Fiber Orientation on Cockling of Paper*. PhD thesis, University of Kuopio, 2007.

[3] Jack R. Vinson. *The Behavior of Sandwhich Structures of Isotropic and Composite Materials*. Technomic, 1999.

[4] Petri Kere and Mikko Lyly. Reissner-Mindlin-Von Kármán type plate model for nonlinear analysis of laminated composite structures. *Computers and Structures*, 86(9):1006–1013, 2008.

[5] Stephen P. Timoshenko and S. Woinowsky-Krieger. *Theory of Plates and Shells*. McGraw-Hill, 1959.

[6] Ferdinando Auricchio, Carlo Lovadina, and Elio Sacco. Analysis of mixed finite elements for laminated composite plates. *Comp. Methods Appl. Mech. Engrg*, 190:4767–4783, 2001.

[7] Mikko Lyly, Jarkko Niiranen, and Rolf Stenberg. A refined error analysis of MITC plate elements. *Mathematical Models and Methods in Applied Sciences*, 16(7):967–977, 2006.

[8] Franco Brezzi, Michel Fortin, and Rolf Stenberg. Error analysis of mixed-interpolated elements for Reissner-Mindlin plates. *Mathematical Models and Methods in Applied Sciences*, 2:125–151, 1991.

[9] Roger A. Horn and Charles R. Johnson. *Matrix Analysis*. Cambridge University Press, 1985.

[10] Franco Brezzi, Klaus-Jürgen Bathe, and Michel Fortin. Mixed-interpolated elements for Reissner-Mindlin plates. *Internat. J. Numer. Methods Engrg.*, 28(8):1787–1801, 1989.

[11] Mikko Lyly, Rolf Stenberg, and Teemu Vihinen. A stable bilinear element for the Reissner-Mindlin plate model. *Comput. Methods Appl. Mech. Engrg.*, 110(3-4):343–357, 1993.

[12] Mikko Lyly. On the connection between some linear triangular Reissner-Mindlin plate bending elements. *Numer. Math.*, 85(1):77–107, 2000.

[13] Juho Könnö. Finite element analysis of composite laminates (in Finnish). Master's thesis, Helsinki University of Technology, 2007.

[14] Douglas N. Arnold and Richard S. Falk. A uniformly accurate finite element method for the Reissner-Mindlin plate. *SIAM Journal on Numerical Analysis*, 26:1276–1290, 1989.

[15] Dietrich Braess. *Finite Elements*. Cambridge University Press, 2001.

[16] P Lipponen, T Leppänen, J Kouko, and J Hämäläinen. Elasto-plastic approach for paper cockling phenomenon: On the importance of moisture gradient. *International Journal of Solids and Structures*, 45:3596–3609, 2008.

[17] M Htun and C Fellers. The invariant mechanical properties of oriented handsheets. *TAPPI journal*, 65:113–117, 1982.

[18] Numerola Oy. `http://www.numerola.fi`, 2008.

(continued from the back cover)

A550 István Faragó, Róbert Horváth, Sergey Korotov
Discrete maximum principles for FE solutions of nonstationary diffusion-reaction problems with mixed boundary conditions
August 2008

A549 Antti Hannukainen, Sergey Korotov, Tomás Vejchodský
On weakening conditions for discrete maximum principles for linear finite element schemes
August 2008

A548 Kalle Mikkola
Weakly coprime factorization, continuous-time systems, and strong-H^p and Nevanlinna fractions
August 2008

A547 Wolfgang Desch, Stig-Olof Londen
A generalization of an inequality by N. V. Krylov
June 2008

A546 Olavi Nevanlinna
Resolvent and polynomial numerical hull
May 2008

A545 Ruth Kaila
The integrated volatility implied by option prices, a Bayesian approach
April 2008

A544 Stig-Olof Londen, Hana Petzeltová
Convergence of solutions of a non-local phase-field system
March 2008

A543 Outi Elina Maasalo
Self-improving phenomena in the calculus of variations on metric spaces
February 2008

A542 Vladimir M. Miklyukov, Antti Rasila, Matti Vuorinen
Stagnation zones for A-harmonic functions on canonical domains
February 2008

HELSINKI UNIVERSITY OF TECHNOLOGY INSTITUTE OF MATHEMATICS
RESEARCH REPORTS

The reports are available at *http://math.tkk.fi/reports/* .
The list of reports is continued inside the back cover.

A560 Sampsa Pursiainen
Computational methods in electromagnetic biomedical inverse problems
November 2008

A554 Lasse Leskelä
Stochastic relations of random variables and processes
October 2008

A553 Rolf Stenberg
A nonstandard mixed finite element family
September 2008

A552 Janos Karatson, Sergey Korotov
A discrete maximum principle in Hilbert space with applications to nonlinear cooperative elliptic systems
August 2008

A551 István Faragó, Janos Karatson, Sergey Korotov
Discrete maximum principles for the FEM solution of some nonlinear parabolic problems
August 2008

ISBN 978-951-22-9600-2 (print)
ISBN 978-951-22-9601-9 (PDF)
ISSN 0784-3143 (print)
ISSN 1797-5867 (PDF)